Excitation-autoionization contributions to the electron-impact ionization of Kr^{4+}–Kr^{7+}

T. W. Gorczyca and M. S. Pindzola
Department of Physics, Auburn University, Auburn, Alabama 36849

N. R. Badnell
Department of Physics and Applied Physics, University of Strathclyde, Glasgow, G4 0NG, United Kingdom

D. C. Griffin
Department of Physics, Rollins College, Winter Park, Florida 32789
(Received 12 October 1993)

We report on calculations for the electron-impact ionization of the krypton ions Kr^{4+}–Kr^{7+}. Results are first obtained from a configuration-average distorted-wave calculation. Multiplet-resolution and channel-coupling effects are investigated using an LS-coupled nonrelativistic R-matrix method for the excitation autoionization of Kr^{6+} and Kr^{7+}, and the inclusion of resonance effects is discussed. Term dependence and relaxation effects, which are found to be significant, are incorporated through the use of pseudo-orbitals. These R-matrix results are found to be in good agreement with LS-coupled distorted-wave calculations. Final results for the excitation-autoionization contributions for Kr^{6+} and Kr^{7+} are obtained in a semirelativistic intermediate-coupled distorted-wave approximation, including both term dependence and relaxation effects. Comparison to experiment is made where available.

PACS number(s): 34.80.Kw

I. INTRODUCTION

Electron-impact ionization of rare-gas ions is an important process occurring in hot plasmas such as those encountered in controlled thermonuclear fusion research. Modeling the physics in these systems requires reliable theoretical collision cross sections to determine the ionization equilibrium and to obtain temperature and density information about the plasma [1]. Krypton is introduced as a diagnostic impurity for the central core, as a source of electrons for studies of the edge plasma, and as a radiation "coolant" for diverters. Thus accurate cross sections at all ionization stages of the krypton isonuclear sequence are required.

To date there have been a small number of such cross sections measured and calculated for various krypton ions. Tinschert *et al.* measured ionization cross sections for the ions Kr^{+}–Kr^{3+} [2]. They found that the parametrized Lotz formula [3, 4] for direct ionization out of the $4p$ subshell adequately reproduced their experimental results. Several other measurements have arrived at similar conclusions [5–9]. Bannister *et al.* [10] performed measurements for ionization of Kr^{8+} and found good agreement with distorted-wave calculations for direct ionization out of the $3d$ subshell. In these four cases the outer subshell has a high occupation number, so that direct ionization is expected to be the dominant process.

However, when the target configuration consists of a singly or doubly occupied outer shell outside of an inner shell with a large occupation number, indirect processes involving inner-shell excitation can become quite important. Recently, Chen and Reed [11] calculated electron-impact ionization cross sections for Kr^{24+} and Kr^{25+} using a relativistic distorted-wave method. They noticed a dominant contribution from inner-shell excitation autoionization of the form $2p \rightarrow 3l$ and also significant enhancement due to resonant excitation of the form $2pkl \rightarrow 4l'nl''$ followed by double autoionization. The target configurations are $2p^6 3s$ and $2p^6 3s^2$ for Kr^{25+} and Kr^{24+}, respectively, which satisfy the requirements noted above for likelihood of strong indirect effects. Similar effects were noticed for Li-like, Be-like, and B-like Kr^{31+}–Kr^{33+} [12], although direct ionization was dominant in these cases.

Another region of the isonuclear sequence where indirect effects may be substantial is around Kr^{17+}, which has a target configuration of $3p^6 3d$. R-matrix calculations for the lower members of this isoelectronic sequence, particularly Ca^{+} [13], Sc^{2+} [14], and Ti^{3+} [15], have shown that $3p^6 3d \rightarrow 3p^5 3d^2$ excitation autoionization dominates the ionization process in the threshold region. For ions more than three-times ionized, however, the $3p^5 3d^2$ terms are bound, so that the indirect contributions arise from the weaker $\Delta n > 0$ transitions. Furthermore, for highly charged Kr^{17+}, relativistic and radiation-damping effects must be included.

A third region where large excitation-autoionization and resonant-excitation double-autoionization features might be expected is in the isonuclear sequence Kr^{4+}–Kr^{7+}. The $3d^{10}4s$ ground state of Kr^{7+}, for instance, contains only a single electron outside of ten $3d$-subshell electrons. These ions are fairly low charged as well, meaning that radiation damping effects are not expected to be important, but channel-coupling effects could be. In this paper we carry out calculations for electron-impact ionization of these four krypton ions and investi-

gate the significance of channel coupling, multiplet resolution within a configuration, and term-dependence effects on the inner-shell excitation-autoionization contribution to the total cross section for just Kr^{6+} and Kr^{7+}.

The rest of the paper is organized in the following manner. In Sec. II we briefly describe and compare the different theoretical methods that we use. We then present results of configuration-averaged distorted-wave calculations for all four krypton ions in Sec. III. In Sec. IV we study the $3d \rightarrow 4d$ inner-shell excitation of Kr^{6+} using both R-matrix and distorted-wave methods in the LS-coupling scheme. The same is done for Kr^{7+} in Sec. V. Section VI describes our intermediate-coupled distorted-wave calculations for the excitation-autoionization contributions in Kr^{6+} and Kr^{7+}, followed by a brief summary in Sec. VII.

II. THEORETICAL METHODS

The direct-ionization cross section is calculated with a configuration-average distorted-wave method [16, 17] which uses partial-wave expansions for the incident, scattered, and ejected electrons. These results are then added incoherently to the indirect excitation cross sections, which are determined from either a distorted-wave or close-coupling method. The branching ratios for autoionization are approximately one for Kr^{4+} to Kr^{7+}.

The first method we use to calculate the inner-shell excitation cross sections is the configuration-average distorted-wave (DWCA) approximation [17, 18], which averages over the various LS terms arising from a given excited configuration. The orbitals needed to describe the target ion are obtained using the Hartree-Fock relativistic code of Cowan [19]. This method includes relativistic corrections and can account for relaxation of the core orbitals by using a different basis for the ground and excited configurations. It is a computationally inexpensive method for the determination of the cross sections to various autoionizing configurations. The major source of error in this method comes from the fact that the LS terms within a configuration, which may be numerous and may have strikingly different characteristics, are approximated by a single configuration excitation.

We can account for the structure of a configuration by explicitly including the various LS terms as target states. One way to do this is to use a distorted-wave LS-coupled (DWLS) method [20]. In this approximation, excitation from the ground state to each excited term is allowed, but the coupling effects between these terms is ignored. For highly charged ions this coupling is negligible due to the dominant Coulomb potential [20, 21], but it is not clear how important such an effect is in the region of ionization we are studying. Also absent from a DWLS formulation is the inclusion of resonance effects, which can contribute to the excitation cross section through resonant-excitation double autoionization. Although the distorted-wave method can be used in conjunction with atomic structure calculations for the $(N+1)$-electron resonance states, leading to the independent-processes isolated-resonance distorted-wave (IPIRDW) approximation [22,23], this approach does not account for interacting-resonance phenomena, which in certain cases can be significant [24].

To fully include channel-coupling and resonance effects, we solve the close-coupling equations using the R-matrix method [25] as coded for the opacity project [26]. The multiconfiguration Hartree-Fock (MCHF) program of Froese Fischer [27] is employed to produce target orbitals for input to the R-matrix codes. One advantage of this method is that we can construct and use pseudo-orbitals which are needed to properly account for term dependence within a LS multiplet.

We have also made adjustments in the angular weights portion of the R-matrix code [28] so that the exact same method for generating angular coefficients for the R-matrix calculations are used for the DWLS method as well. This required a restructuring of the program to produce as output only those coefficients that are required by the DWLS code. In this part of the R-matrix calculation, the angular coefficients are normally calculated for bound-bound, bound-continuum, and continuum-continuum Hamiltonian matrix elements. Since the present DWLS method does not use any $(N+1)$-electron bound wave functions, we have omitted all but the continuum-continuum part of the calculation when using the R-matrix code to generate these coefficients. For complex systems, the angular coefficients involved in the bound portion of the total wave function can be more extensive than those involved in the continuum portion, so that omitting the bound-bound and bound-continuum algebra leads to a substantial reduction in computational effort. Using the same method for generating angular coefficients and the same bound-state orbitals for both the R-matrix and DWLS calculations helps guarantee a consistent comparison between the two methods.

We now point out some of the differences between these last two computational methods. First of all, the DWLS method does not orthogonalize the continuum solutions to the bound orbitals. Because of this, we must augment the off-diagonal potential interaction terms with energy-dependent exchange-overlap terms. However, it is not necessary to use the same set of orbitals to describe the individual LS terms, and as such we can easily account for the various relaxation and term-dependent effects [19, 29] that may exist. The R-matrix method, on the other hand, imposes orthogonality between all orbitals, both continuum and bound, in order to simplify the evaluation of Hamiltonian matrix elements [25]. This condition requires that each LS target term is described by the same set of orbitals. It also necessitates the inclusion of $(N+1)$-electron bound configurations to compensate for the enforced orthogonality of the continuum orbitals to the bound ones [25]. The first of these two restrictions makes it difficult to account for orbital differences between various target terms; the second leads to pseudo-resonance effects in certain cases. We shall address these points with specific examples in Sec. IV.

The R-matrix method properly accounts for channel-coupling effects, however, and implicitly incorporates resonance effects as well. It is therefore an essential method for investigating the importance of these effects when compared to the DWLS method. For this reason, we use

the same target description for the DWLS and R-matrix methods even though we are free to use different sets of orbitals for the DWLS calculations. We remark that the R-matrix treatment fails to include radiation damping of resonances, which the IPIRDW method handles in a straightforward manner, but this was found to be small for the stages of ionization we are presently studying.

III. CONFIGURATION-AVERAGE DISTORTED-WAVE RESULTS FOR KR^{4+}–KR^{7+}

As a first step, we performed DWCA calculations for the electron-impact excitation autoionization of the sequence Kr^{4+}–Kr^{7+}. These indirect results are added to distorted-wave direct-ionization results to obtain the total-ionization cross section. We show these results for Kr^{4+} in Fig. 1. The thresholds for these various ionization and excitation processes, as well as pertinent cross section magnitudes, are listed in Table I. We note that direct ionization of the $3d$ electron is not included in Fig. 1. This is because the resulting $3d^9 4p^2$ configuration of Kr^{5+} will autoionize to the $3d^{10}$ configuration of Kr^{6+} and thus contribute to the double-ionization cross section of Kr^{4+}. Also shown in Fig. 1 are the crossed-beams experimental results of Bannister *et al.* [30] presented in the preceding paper. The theoretical and experimental results show the same general behavior throughout the entire energy range. Nevertheless, there are certain noticeable discrepancies between the two. First of all, the experimental data show a non-zero cross section below the first-ionization threshold, indicating that metastable ions may be present in the ion beam. This could account for some of the difference in the near-threshold region. More importantly, perhaps, is the fact that the DWCA method does not include any resonant-excitation double-autoionization contributions in this threshold region. Including such effects would lead to an extremely involved calculation due to the complex structure of these configurations. As can be seen from Table I, the dominant contribution to the cross section is the $3d \rightarrow 4d$ inner-shell excitation. Performing a complete LS-coupled R-matrix calculation for this transition alone would require the 100 LS target terms associated with the $3d^9 4s^2 4p^2 4d$ configuration to be included in the close-coupling expansion.

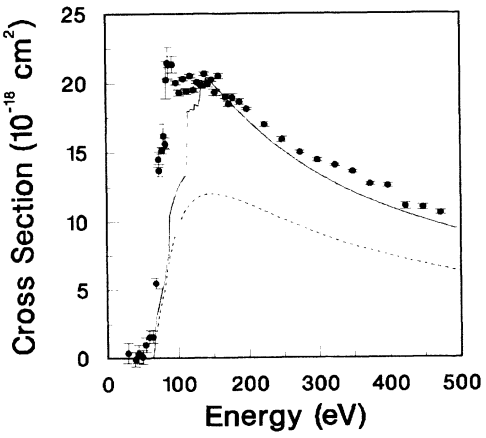

FIG. 1. Electron-impact ionization cross section for Kr^{4+}. Dashed curve, direct-ionization contribution, full curve, configuration-average distorted-wave excitation results added to the direct cross section, solid circles, experimental measurements (Ref. [30]).

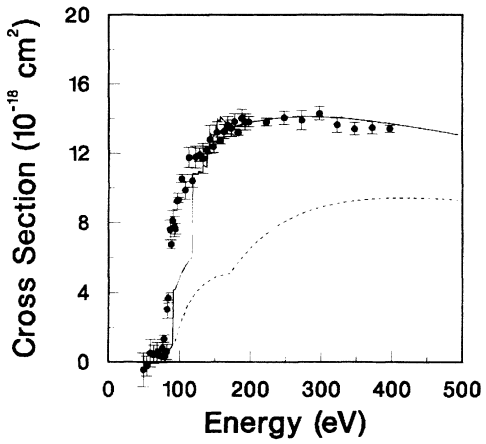

FIG. 2. Electron-impact ionization cross section for Kr^{5+}. Dashed curve, direct-ionization contribution, full curve, configuration-average distorted-wave excitation results added to the direct cross section, solid circles, experimental measurements (Ref. [30]).

For ionization of Kr^{5+} we show our results in Table II and Fig. 2, where the $3d$ direct ionization contribution is now included. The agreement between theory and experiment is quite good, and the excitation-autoionization enhancement is more prominent for this ion than for Kr^{4+}. The $3d \rightarrow 4d$ transition is responsible for the largest contribution. As noted earlier, we expect an increase in the importance of indirect effects as the number of $4p$ electrons outside the $3d$ subshell decreases. This general trend is apparent as we proceed along the isonuclear sequence to the ionization of Kr^{6+}. We show the results of this calculation in Fig. 3 and Table III. The excitation-

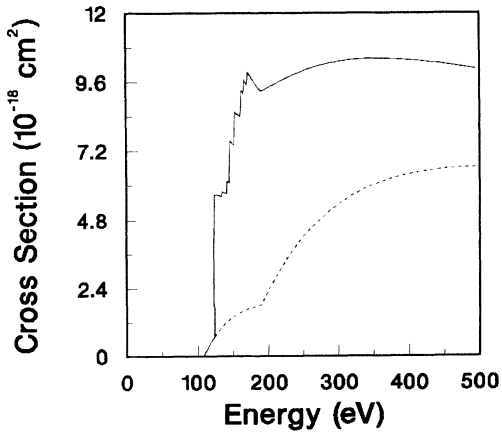

FIG. 3. Electron-impact ionization cross section for Kr^{6+}. Dashed curve, direct-ionization contribution, full curve, configuration-average distorted-wave excitation results added to the direct cross section.

TABLE I. Configuration-average ionization and excitation cross sections for Kr^{4+}.

Subshell	Ionization potential (eV)	Cross section at twice threshold (Mb)
	Ionization	
$4p$	63.41	8.10
$4s$	79.77	3.99
$3d$	153.46	5.56
Transition	**Excitation energy (eV)**	**Cross section at threshold (Mb)**
	Excitation	
$4s \rightarrow 6s$	60.21	1.45
$4s \rightarrow 6p$	62.58	0.94
$4s \rightarrow 6d$	66.31	0.99
$3d \rightarrow 4p$	86.86	2.50
$3d \rightarrow 4d$	112.37	4.48
$3d \rightarrow 4f$	130.51	0.47
$3d \rightarrow 5p$	123.68	0.43
$3d \rightarrow 5d$	131.79	1.02
$3d \rightarrow 5f$	138.92	0.31
$3d \rightarrow 6p$	136.02	0.16
$3d \rightarrow 6d$	139.79	0.44
$3d \rightarrow 6f$	143.45	0.19

TABLE II. Configuration-average excitation and ionization cross sections for Kr^{5+}.

Subshell	Ionization potential (eV)	Cross section at twice threshold (Mb)
	Ionization	
$4p$	77.76	2.46
$4s$	93.55	2.68
$3d$	171.34	5.11
Transition	**Excitation energy (eV)**	**Cross section at threshold (Mb)**
	Excitation	
$3d \rightarrow 4p$	90.05	3.08
$3d \rightarrow 4d$	117.53	4.76
$3d \rightarrow 4f$	138.35	0.94
$3d \rightarrow 5p$	132.55	0.44
$3d \rightarrow 5d$	141.95	1.12
$3d \rightarrow 5f$	150.43	0.55
$3d \rightarrow 6p$	148.03	0.16
$3d \rightarrow 6d$	152.55	0.48
$3d \rightarrow 6f$	156.94	0.32

TABLE III. Configuration-average excitation and ionization cross sections for Kr^{6+}.

Subshell	Ionization potential (eV)	Cross section at twice threshold (Mb)
	Ionization	
$4s$	107.93	1.91
$3d$	190.21	4.60
Transition	**Excitation energy (eV)**	**Cross section at threshold (Mb)**
	Excitation	
$3d \rightarrow 4p$	93.58	3.48*
$3d \rightarrow 4d$	122.91	4.93
$3d \rightarrow 4f$	145.78	1.47
$3d \rightarrow 5p$	141.75	0.43
$3d \rightarrow 5d$	152.34	1.18
$3d \rightarrow 5f$	162.00	0.78
$3d \rightarrow 6p$	160.46	0.16
$3d \rightarrow 6d$	165.69	0.50
$3d \rightarrow 6f$	170.76	0.44

TABLE IV. Configuration-average excitation and ionization cross sections for Kr^{7+}.

Subshell	Ionization potential (eV)	Cross section at twice threshold (Mb)
	Ionization	
$4s$	125.54	0.70
$3d$	211.16	4.05
Transition	**Excitation energy (eV)**	**Cross section at threshold (Mb)**
	Excitation	
$3d \rightarrow 4p$	99.31	3.05*
$3d \rightarrow 4d$	129.09	5.05
$3d \rightarrow 4f$	153.79	2.03
$3d \rightarrow 5p$	152.24	0.39
$3d \rightarrow 5d$	163.94	1.19
$3d \rightarrow 5f$	174.63	1.00
$3d \rightarrow 6p$	174.36	0.15
$3d \rightarrow 6d$	180.27	0.50
$3d \rightarrow 6f$	185.94	0.55

autoionization process now dominates the total cross section in the threshold region, due mostly to the $3d \rightarrow 4d$ excitation again. For this reason we will look more closely at this excitation process in Sec. IV in order to study the channel-coupling and multiplet-resolution effects not included in the DWCA calculations.

The ionization cross sections for Kr^{7+} are listed in Table IV and plotted in Fig. 4, along with the experimental data [30]. In the threshold region we see an order of magnitude enhancement over the direct cross section due to the indirect $3d \rightarrow 4d$ excitation-autoionization process. These DWCA results show a much more dramatic rise in cross section than the experimental data, however. This discrepancy is mostly due to describing the $3d^9 4s4d$ configuration by a single excitation level. The effects of resolving this configuration into separate LS multiplets and the effects of channel coupling will be investigated in the paragraphs below.

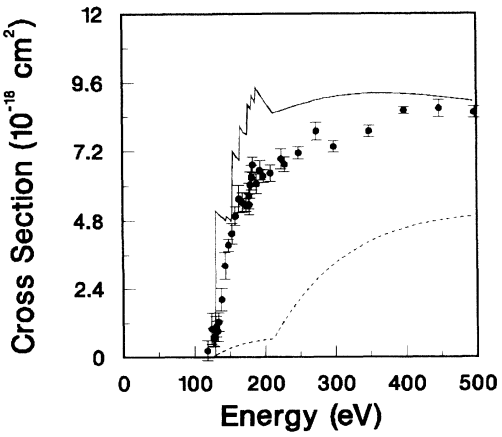

FIG. 4. Electron-impact ionization cross section for Kr^{7+}. Dashed curve, direct-ionization contribution, full curve, configuration-average distorted-wave excitation results added to the direct cross section, solid circles, experimental measurements (Ref. [30]).

IV. LS-COUPLED CALCULATIONS FOR Kr^{6+}

As shown in the preceding section, $3d \rightarrow 4d$ excitation-autoionization dominates the ionization process for Kr^{6+}. We further investigate this transition by explicitly including the ten LS terms associated with the $3d^9 4s^2 4d$ excited configuration in the target expansion and apply DWLS and R-matrix treatments to the problem.

A. Choice of atomic basis

We first performed term-dependent Hartree-Fock (TDHF) calculations for each of the individual terms separately. These results are listed in Table V. Although further configuration-interaction (CI) mixing with configurations of the form $3d^{10}4p^2$ and $3d^9 4p^2 4d$ was found to be important in order to fully describe these terms, such effects are negligible compared to the inaccuracies introduced by using a single orthogonal basis as discussed below. Furthermore, the inclusion of such complex configurations in the target description leads to a more involved R-matrix calculation.

We next calculated the CI energies obtained using various sets of orbitals. The natural choice for a single orthogonal basis is the $1s2s...3d4s$ orbitals obtained from a TDHF calculation for the ground state, and a $4d$ orbital determined from a frozen-core HF calculation for the average energy of the $3d^9 4s^2 4d$ configuration. This basis is referred to as GO+$4d$ (ground-state orbitals plus $4d$), and the resulting CI energies for this basis are listed in Table V. Note that two main discrepancies exist between the TDHF values and those obtained with this basis. First, the CI energies of the nine lowest excited LS terms are roughly 3.5 eV above the corresponding TDHF values. This is primarily due to relaxation effects in the $3d$ and $4s$ orbitals, the $3d$ relaxation being much more significant. In the ground configuration, the $3d$ subshell is occupied by ten electrons, leading to an effective shielding by nine other $3d$ electrons. In the excited configuration, on the other hand, the $3d$ orbital is shielded by only eight other $3d$ electrons, and so it is "relaxed," or

TABLE V. Hartree-Fock and CI energies of Kr^{6+} (eV).

LS term	TDHF[a]	CI basis		
		GO+4d[a]	RO+5d[b]	RO+$\overline{5d}$[c]
$3d^{10}4s^2\,{}^1S$	0.000	0.000	0.000	0.000
$3d^9 4s^2 4d\,{}^3S$	122.472	125.847	120.605	121.784
${}^3G$	123.732	127.206	121.809	123.033
${}^1P$	123.821	127.319	121.896	123.122
${}^3P$	124.821	127.319	121.896	123.122
${}^1G$	124.060	127.603	122.132	123.361
${}^3D$	124.125	127.637	122.198	123.426
${}^1F$	124.651	128.242	122.725	123.952
${}^3F$	124.651	128.242	122.725	123.952
${}^1D$	124.878	128.592	122.965	124.182
${}^1S$	130.164	140.998	132.244	131.090

[a] Relative to TDHF ground-state energy=−2742.461 a.u.

[b] Relative to CI ground-state energy=−2742.390 a.u. (1.932 eV above the TDHF value).

[c] Relative to CI ground-state energy=−2742.435 a.u. (0.708 ev above the TDHF value).

more tightly bound, compared to the same orbital in the ground configuration. Since we have used a basis containing the ground 3d and 4s orbitals to describe these excited terms rather than the proper excited orbitals, the resultant energies are higher than the TDHF values.

The second difference between the two results is that the ${}^1S$ excited-term energy is almost 11 eV above the TDHF value. In addition to the approximately 3.5 eV shift just described, this inaccuracy is also due to term dependence [19, 29] of the 4d orbital. The strong 3d-4d repulsive exchange potential which is present primarily for this term yields a TDHF 4d(${}^1S$) orbital which resides at a larger radius than the 4d orbitals for the other nine LS terms. Using the configuration-average 4d orbital to describe this ${}^1S$ term causes a large error in the threshold energy value. More importantly, relaxation and term dependence errors can lead to inaccuracies in the excitation cross sections, as shown below.

One way to partially correct this term dependence problem is to allow CI mixing between the $3d^9 4s^2 4d$ and $3d^9 4s^2 5d$ configurations, so that the 4d orbital for the ${}^1S$ state is now represented by a weighted sum of the configuration-average 4d and 5d orbitals. Relaxation of the 3d orbital, on the other hand, can be accounted for by using a basis set composed of orbitals determined from a HF calculation for the average energy of the excited $3d^9 4s^2 4d$ configuration, thereby giving a more accurate description for the excited terms. This leads to an inaccuracy in the $3d^{10}4s^2$ ground-state energy instead, but this inaccuracy is approximately corrected by CI mixing with the $3d^9 4s^2 4d$ and $3d^9 4s^2 5d$ configurations. The basis just described will be referred to as RO+5d (relaxed orbitals + 5d orbital) and the resulting CI energies are listed in Table V. The CI ground-state energy for this basis is almost 2 eV above the TDHF value, so that there is an appreciable error in the ground-state description, and this leads to shifts of about 2 eV in the thresholds for the nine lowest excited LS terms. Even with this 2 eV shift, the ${}^1S$ excited LS term is still more than 2 eV above the full TDHF value, showing that the 4d term dependence is not fully accounted for by using just a single 5d orbital.

To further incorporate term-dependent effects of the 4d orbital in the ${}^1S$ state, we could include CI mixing with the $3d^9 4s^2 6d$ configuration, and so on. This requires an even larger R-matrix region to contain the 6d orbital, leading to a more difficult calculation, and this additional orbital only partially corrects for term dependence. A more straightforward way is to use just one $\overline{5d}$ pseudo-orbital, which does not correspond to any one physical nd orbital, but rather is determined from a MCHF calculation for the ${}^1S$ excited state using the $3d^9 4s^2 4d$ and $3d^9 4s^2 \overline{5d}$ configurations, where all other orbitals are frozen. This pseudo-orbital then corrects the ${}^1S$ term dependence of the 4d orbital exactly. The CI energies resulting from this RO+$\overline{5d}$ basis are listed in Table V, showing that the energies of each LS term are within 1 eV of the respective TDHF values. The remaining discrepancy is primarily due to error in the energy of the $3d^{10}4s^2$ ground state term.

B. Excitation cross sections

We first investigate multiplet resolution within the $3d^9 4s^2 4d$ configuration by comparing DWCA and DWLS calculations for just the $3d \rightarrow 4d$ excitation. The DWCA method includes relativistic corrections and uses a different set of orbitals for the ground and the excited configurations. The DWLS method, on the other hand, lacks any relativistic effects, and we have chosen to use a single set of orbitals (the GO+4d basis) since we will be comparing to the R-matrix method below. The results of these two calculations are shown in Fig. 5. Although the DWLS threshold results are shifted upward in energy due to the omission of relaxation effects, the cross sections just above the final threshold are quite similar in both cases. It is apparent that the main contribution to the cross section is from excitation to the uppermost ${}^1S$ term, and since this term is poorly described by a configuration-average 4d orbital, there may be a large

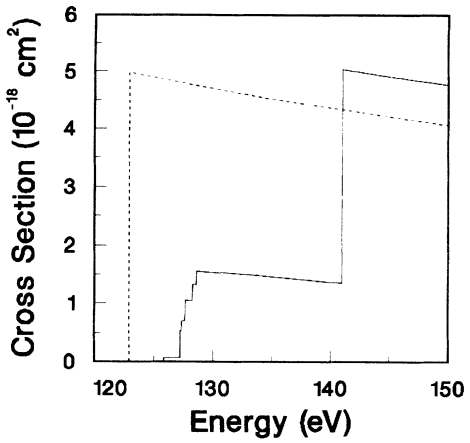

FIG. 5. $3d \rightarrow 4d$ excitation cross sections for Kr^{6+}. Solid curve, LS-coupled distorted-wave results using the GO+4d basis, dashed curve, configuration-average distorted-wave results.

error in this particular excitation cross section.

We can also investigate the importance of interchannel coupling by comparing the DWLS and R-matrix methods for the $3d \rightarrow 4d$ excitation using the same GO+4d basis. These results are shown in Fig. 6, and it can be seen that coupling effects are not significant by noting that the background R-matrix results are almost identical to the DWLS results, the main difference between the two being the resonance contributions which are inherent in the R-matrix calculation. These resonance effects, which are not too strong in this case, will be discussed later in this section.

Section IV A, regarding the target description, illustrated that term dependence and relaxation effects cause inaccuracies in the various threshold energies due to the limitations of using a single basis. This alone does not pose any great problem since it is possible to adjust the thresholds before performing the actual scattering calculations [31]. However, the use of a poor target orbital also causes inaccuracies in the interaction potential, and therefore in the excitation cross section. To see this, we now compare excitation cross sections obtained using different bases. The results of an R-matrix calculation using the RO+5d target basis are plotted in Fig. 7, and it can be seen that several differences exist between these results and those obtained by using the GO+4d basis (Fig. 6). As shown in Table V and discussed above, the thresholds are lower in energy for three reasons. First, relaxed $3d$ and $4s$ orbitals are used, so that the absolute energy of the nine lowest excited terms will be more accurate. Second, because the relaxed orbitals are used, the ground-state absolute energy is greater than the correct ground-state energy, which leads to even lower relative energies of the excited states. Third, CI mixing between the $4d$ and $5d$ orbitals allows an approximate, but not full, correction for term dependence in the excited ^1S term. These RO+5d threshold energies are therefore inadequate, and furthermore the excitation cross section to the ^1S term is only slightly reduced compared to that obtained with the GO+4d basis. When the RO+$\overline{5d}$ basis is used, the excited thresholds are fairly accurate; more importantly, since the excited ^1S term is now properly described, the excitation cross section to this term is much smaller than the previous two cases (Fig. 8). Thus the strong term dependence of the $4d$ orbital must be accounted for not only to obtain the correct excited ^1S threshold, but also to obtain the correct threshold cross section.

By comparing the DWLS and R-matrix results in Fig. 6, we determined that channel-coupling effects were small for this case. But the same comparison in Fig. 8 seems to suggest that coupling becomes more important when using the more complex RO+$\overline{5d}$ basis. This discrepancy is due to the existence of pseudo-resonances in the above-threshold region arising from $3d^9\overline{5d}^2$ $(N+1)$-electron configurations which interfere with the background cross section. These states must be included in the total wave

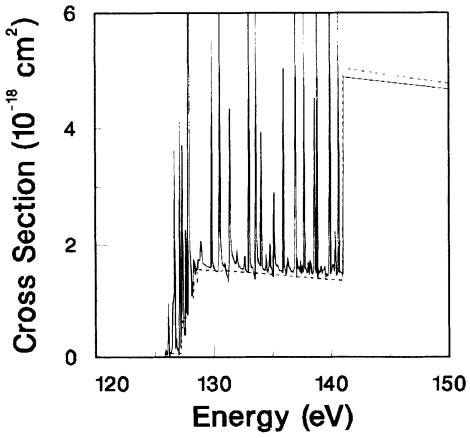

FIG. 6. Excitation cross section to all ten $3d^9 4s^2 4d$ LS terms of Kr^{6+} using the GO+4d basis. Solid curve, 11-state R-matrix calculation, dashed curve, LS-coupled distorted-wave results.

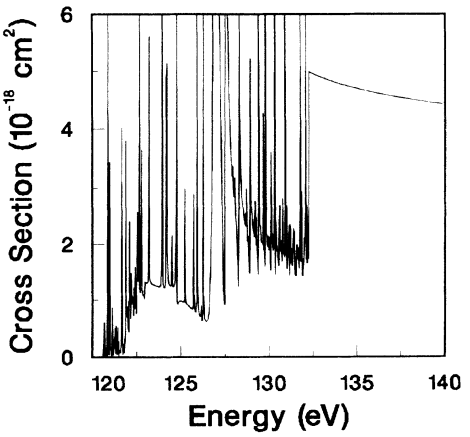

FIG. 7. Excitation cross section to all ten $3d^9 4s^2 4d$ LS terms of Kr^{6+} using the RO+5d basis. Solid curve, 11-state R-matrix calculation.

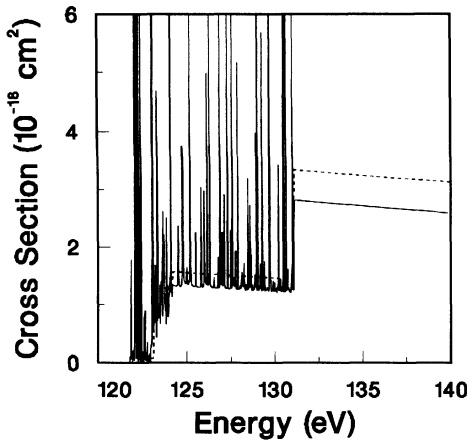

FIG. 8. Excitation cross section to all ten $3d^9 4s^2 4d$ LS terms of Kr^{6+} using the RO+$\overline{5d}$ basis. Solid curve, 11-state R-matrix calculation, dashed curve, LS-coupled distorted-wave results.

function expansion to compensate for the combined situation that first, the target states include some admixture of the $3d^9 4s^2 \overline{5d}$ configuration in their description and second, the continuum orbitals are orthogonalized to the $\overline{5d}$ pseudo-orbital. While these pseudoresonances are not physically meaningful, it is not clear how these can be eliminated without removing a necessary contribution to the continuum channel description.

Another point concerning these resonances should be made. As shown in studies of the isoelectronic sequence Ca^+ [13], Sc^{2+} [14], and Ti^{3+} [15], inclusion of singly excited states in the close-coupling expansion significantly decreases the resonance contributions to the total cross section. This is because including the singly excited states in the target expansion provides alternate decay channels for the doubly excited resonances. We found this same effect in calculations of inner-shell excitation to the six nonautoionizing terms of the $3d^9 4s^2 4p$ configuration in Kr^{6+}. When singly excited target states of the type $3d^{10} 4snl$ were included, the resonance contributions decreased. These resonances can also radiatively decay to bound terms of the Kr^{5+} ion, although this was found to be a small effect in the present case. This radiative process, which is routinely incorporated in the IPIRDW method, is not accounted for within the standard formulation of the R-matrix method.

A third consideration in the proper description of resonances is the inclusion of higher-lying $3d^9 nln'l'$ target configurations leading to resonances of the form $3d^9 nln'\ell' n''l''$. While these target states are necessary in order to properly describe resonance contributions, doing so would require an extremely involved R-matrix calculation owing to the large number of channels obtained from these configurations.

Due to the possible sources of error described above, care must be exercised in using the R-matrix method to describe resonant processes in complex low-charged ions. In particular, a sufficient number of LS terms must be included in the close-coupling expansion in order to insure that all pertinent resonance contributions have been accounted for. One should also be aware of the anomalous effects of pseudoresonances. A sufficient number of singly excited channels should be included for allowance of alternate decay paths of the resonances. And finally, for higher-charged ions, the effects of radiation damping must be incorporated.

What we have seen in this section is that term dependence and relaxation must be accounted for in order to obtain reliable $3d \rightarrow 4d$ excitation cross sections. Also, DWLS and R-matrix methods gave essentially the same results for the background cross section. The main difference is due to the resonances present

TABLE VI. Hartree-Fock and CI energies of Kr^{7+} (eV).

LS term	TDHF[a]	CI basis	
		GO+4d[a]	RO+$\overline{5d}$[b]
$3d^{10} 4s\,^2S$	0.000	0.000	0.000
$3d^9 4s(^3D) 4d\,^4S$	127.260	130.230	126.820
^4G	128.686	131.825	128.234
^4P	128.794	131.970	128.342
^4D	129.126	132.320	128.673
$3d^9 4s(^1D) 4d\,^2P$	129.353	132.520	128.900
^2G	129.559	132.770	129.108
$3d^9 4s(^3D) 4d\,^4F$	129.725	133.029	129.271
$3d^9 4s(^1D) 4d\,^2S$	130.535	133.147	129.718
^2F	130.282	133.580	129.828
^2D	130.338	133.764	129.935
$3d^9 4s(^3D) 4d\,^2G$	132.035	135.328	131.593
^2P	132.078	135.385	131.634
^2D	132.560	135.995	132.115
^2F	132.963	136.446	132.523
^2S	137.413	149.308	138.558

[a] Relative to the TDHF ground-state energy=−2738.589 a.u.

[b] Relative to the CI ground-state energy=−2738.572 a.u. (0.454 eV above the TDHF value).

in the R-matrix calculation. Since these resonances are not reliable within the present close-coupling expansion, as noted above, we concentrate our attention on the excitation-autoionization contributions for which the distorted-wave method has been shown to be perfectly adequate. This we will do in Sec. VI.

V. LS-COUPLED Kr^{7+} CALCULATIONS

We now apply the same theoretical treatment of the preceding section to the $3d \rightarrow 4d$ inner-shell excitation of Kr^{7+}. In Table VI we list the Hartree-Fock energies of Kr^{7+}, where interterm mixing within the configuration was allowed between terms with the same symmetry. In other words, the energy of the higher-lying ^2S term, for instance, was obtained by first performing a Hartree-Fock calculation for the $3d^9 4s(^3D)4d(^2S)$ term only, thereby obtaining term-dependent orbitals. Then using these orbitals, mixing was allowed with the $3d^9 4s(^1D)4d(^2S)$ term. This procedure was then repeated for the $3d^9 4s(^1D)4d(^2S)$ term energy, and likewise for the eight other doublet terms. Also listed in this table are various single-basis CI results. For the GO+4d basis, the orbitals up to 4s were determined from a TDHF calculation for the $3d^{10}4s$ ground state, and the 4d orbital was determined from a frozen-core HF calculation for the average energy of the $3d^9 4s4d$ configuration. As in the case for Kr^{6+}, use of this basis leads to a roughly 3 eV energy shift of the 14 lowest terms due to relaxation of the 3d orbital. There is a 12 eV energy difference between the TDHF and CI results in the uppermost ^2S term due to term dependence of the 4d orbital. When a relaxed-orbital basis augmented with a $\overline{5d}$ pseudo-orbital is used, however, the CI energies, as seen in Table VI, show much better agreement with the TDHF values since relaxation and term dependence are now included.

The excitation cross sections are again quite sensitive to the choice of basis. A comparison of DWCA and DWLS results is shown in Fig. 9, where the GO+4d basis is used for the DWLS calculation. Again the main contribution to the total cross section comes from excitation to the uppermost ^2S term, which we know is in error due to the lack of term dependence. In Fig. 10 the results of both R-matrix and distorted-wave calculations are shown for the $3d \rightarrow 4d$ excitation autoionization using the GO+4d basis, indicating that channel-coupling effects are quite small. In order to include relaxation and term dependence, we use instead the RO+$\overline{5d}$ basis and obtain the improved results shown in Fig. 11. The difference between DWLS and R-matrix cross sections can again be attributed to the interference of a higher-lying pseudoresonance with the smooth background cross section.

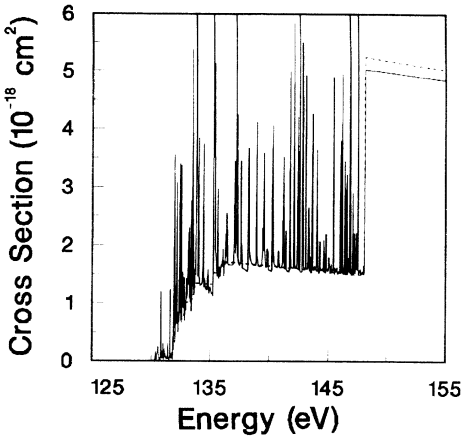

FIG. 10. $3d \rightarrow 4d$ excitation cross sections for Kr^{7+} using the ground-state orbital basis. Solid curve, 16-state R-matrix calculation; dashed curve, LS-coupled distorted-wave results.

VI. INTERMEDIATE-COUPLED DISTORTED-WAVE CALCULATIONS FOR Kr^{6+} AND Kr^{7+}

Sections IV and V have shown that the distorted-wave method is a good approximation for obtaining the back-

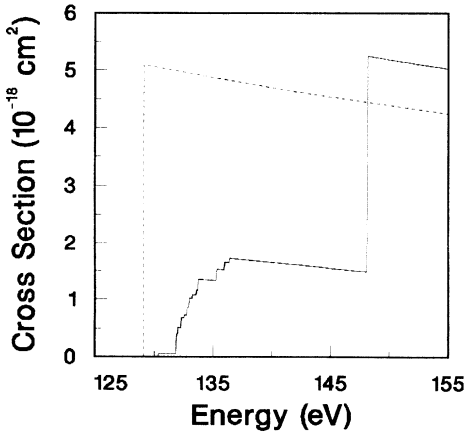

FIG. 9. $3d \rightarrow 4d$ excitation cross sections for Kr^{7+}. Solid curve, LS-coupled distorted-wave results using the ground-state orbital basis, dashed curve, configuration-average distorted-wave results.

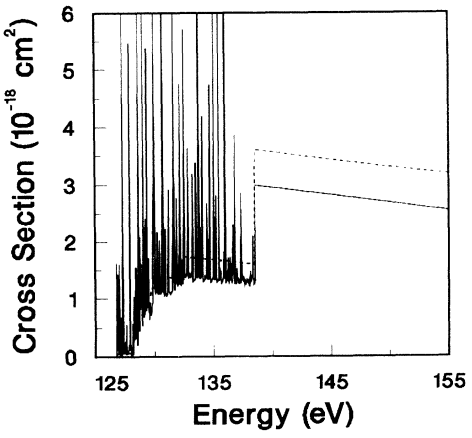

FIG. 11. $3d \rightarrow 4d$ excitation cross sections for Kr^{7+} using the relaxed orbitals and a $\overline{5d}$ pseudo-orbital. Solid curve, 16-state R-matrix calculation; dashed curve, LS-coupled distorted-wave results.

ground excitation-autoionization cross sections for Kr^{6+} and Kr^{7+} provided that term dependence is properly included. However, the previous DWLS calculations omitted relativistic and radiative-decay effects. We therefore have performed intermediate-coupled distorted-wave (DWIC) calculations, as previously described [32–34], in order to obtain the $3d \rightarrow 4d$ and $3d \rightarrow 4f$ excitation-autoionization contributions to the total ionization cross section for both Kr^{6+} and Kr^{7+}. This method uses the Hartree-Fock computer code of Cowan [19], and includes mass-velocity and Darwin relativistic corrections [35], to obtain orbitals for the ground and excited configurations separately. The continuum distorted waves also include relativistic terms within a semiclassical exchange approximation. Branching between autoionization and radiative stabilization is included by calculating the respective Auger and radiative transition rates and computing the proper branching ratios. This was found to be a minor effect for both systems, but these ratios could be altered to correct for term dependence as well, which we describe below.

We first performed DWIC calculations for Kr^{6+}. The $3d \rightarrow 4d$ excitation allowed CI mixing in the final configuration of the form $3d^9 4s^2 4d + 3d^9 4s 4p^2$ so that radiative stabilization to the $3d^{10} 4s 4p$ configuration could occur. The continuum configurations $3d^{10} 4s kl$ (l=1,3,5) were included as Auger decay channels. As noted above, the branching ratios were determined to be close to one for all doubly excited levels, and for the $^1S_{J=0}$ level, this value is identically one. In order to include term dependence, however, this value was modified as follows. We first performed a $3d \rightarrow 4d$ DWLS calculation using a configuration-average $4d$ orbital and obtained a threshold excitation cross section to the $3d^9 4s^2 4d\, ^1S$ term of 3.90 Mb. We then repeated this calculation using a ^1S term-specific $4d$ orbital yielding a reduced cross section of 1.94 Mb. The resulting ratio of 0.5 was used as a multiplicative factor for the excitation cross section to the $3d^9 4s^2 4d\, ^1S_{J=0}$ level in the DWIC calculation. Thus the $4d$ term dependence is included in the $3d \rightarrow 4d$ calculation. For the $3d \rightarrow 4f$ excitation, no CI mixing was required to allow for radiative decay. The $3d^{10} 4s^2$ is present as a radiative decay channel, and the $3d^{10} 4s kl$ (l=1,3,5) configurations allowed for Auger decay. In Fig. 12 we show the DWIC results for the $3d \rightarrow 4d$ and $3d \rightarrow 4f$ transitions, added to the configuration-average distorted-wave direct-ionization cross section [16]. For higher $3d \rightarrow nl$ transistions, the DWCA results were used.

The DWIC calculations for Kr^{7+} were quite similar. The $3d \rightarrow 4d$ calculation included the CI mixing $3d^9 4s 4d + 3d^9 4p^2$ in the final configuration to allow radiative stabilization to the $3d^{10} 4p$ configuration. The Auger channels included were $3d^{10} kl$ (l=0,2,4). The $3d \rightarrow 4f$ calculation included no CI since the excited $3d^9 4s 4f$ configuration is allowed to decay to $3d^{10} 4s$. The Auger states included were $3d^{10} kl$ (l=1,3,5). The branching ratios were nearly unity for all levels, and identically so for the upper $3d^9 4s 4d\, ^2S_{J=1/2}$ level. DWLS calculations for excitation to this term using a configuration-average $4d$ orbital yielded a threshold cross section of 3.08 Mb. The same calculation using a term-specific orbital resulted in a cross section of 1.93 Mb instead, so that a branching ratio of 0.63 was employed as a multiplicative factor for the upper $^2S_{J=1/2}$ level in order to correct for term dependence. These results are shown in Fig. 13. We see that, compared to the DWCA results shown in Fig. 4, the proper inclusion of term dependence within a multiplet-resolved calculation has reduced the ionization cross section so that the theoretical curve is in much better agreement with the experimental results.

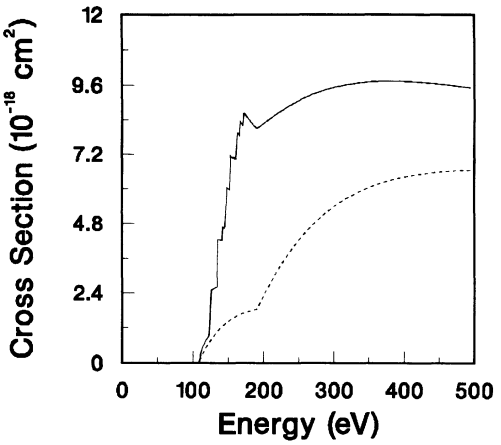

FIG. 12. Electron-impact ionization cross section for Kr^{6+}. Dashed curve, direct-ionization contribution, full curve, intermediate-coupled distorted-wave results for the $3d \rightarrow 4d, 4f$ excitations and configuration-average distorted-wave results for higher $3d \rightarrow nl$ excitations, added to the direct-ionization cross section.

The DWCA results for Kr^{4+}–Kr^{7+}, the DWIC results for Kr^{6+} and Kr^{7+}, and the experimental measurements [30] will be entered into the electronic atomic data base at the Oak Ridge National Laboratory Controlled Fu-

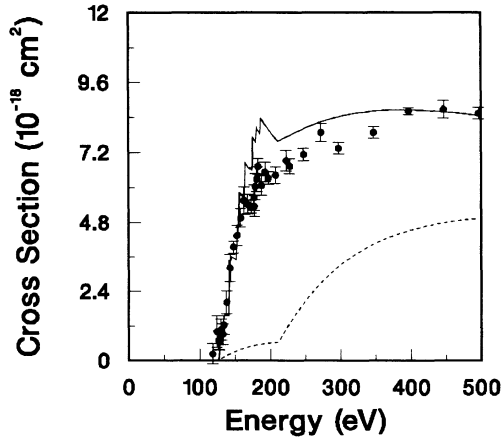

FIG. 13. Electron-impact ionization cross section for Kr^{7+}. Dashed curve, direct-ionization contribution, full curve, intermediate-coupled distorted-wave results for the $3d \rightarrow 4d, 4f$ excitations and configuration-average distorted-wave results for higher $3d \rightarrow nl$ excitations, added to the direct cross section, solid circles, experimental measurements (Ref. [30]).

sion Atomic Data Center and will thus be available via internet to the entire fusion energy community.

VII. CONCLUSION

By studying the electron-impact ionization of the Kr^{4+}–Kr^{7+} sequence, we have shown that the indirect $3d \rightarrow 4d$ excitation-autoionization process is responsible for the dominant contribution to the ionization cross section. Furthermore, this excitation process exhibits strong $4d$ term dependence, as was seen for the Kr^{6+} and Kr^{7+} ions, and relaxation of the 3d orbital must be accounted for to obtain correct threshold energies. By properly including term dependence, the major discrepancy between experimental and configuration-average theoretical results that existed in the near-threshold region for Kr^{7+} was resolved. And by comparing distorted-wave and close-coupling methods, we were able to show that channel-coupling effects are not too important for these transitions.

The present limited R-matrix calculations cannot properly assess the importance of resonances for these ions. The full treatment of resonances within the R-matrix formulation requires a very large expansion in both higher-lying doubly excited states and lower-lying singly excited states. Furthermore, inclusion of term dependence can lead to unphysical pseudo-resonances. Relativistic effects must also be included. The IPIRDW [22–24] method, including interference between resonance structures, may be the most efficient method for including the resonant-excitation double-autoionization contributions.

ACKNOWLEDGMENTS

We would like to thank the members of the Opacity Project for the use of their R-matrix programs. We also thank Mark Bannister for making his experimental results available prior to publication. This work was supported in part by the U.S. Department of Energy, Office of Fusion Energy, under Contract No. DE-FG05-86-ER53217 with Auburn University and Contract No. DE-AC05-84OR21400 with Martin Marietta Energy Systems, Inc.

[1] S. Sudkewer, Phys. Scr. **23**, 72 (1981).
[2] K. Tinschert, A. Müller, G. Hofmann, C. Achenbach, R. Becker, and E. Salzborn, J. Phys. B **20**, 1121 (1987).
[3] W. Lotz, Z. Phys. **216**, 241 (1968).
[4] W. Lotz, Z. Phys. **220**, 466 (1969).
[5] D. C. Gregory, P. F. Dittner, and D. H. Crandall, Phys. Rev. A **27**, 724 (1983).
[6] A. Danjo, A. Matsumoto, S. Ohtani, H. Suzuki, H. Tawara, and K. Wakiya, J. Phys. Soc. Jpn. **53**, 4091 (1984).
[7] D. C. Gregory, Nucl. Instrum. Methods B **10-11**, 87 (1985).
[8] K. F. Man, A. C. H. Smith, and M. F. A. Harrison, J. Phys. B **20**, 5865 (1987).
[9] K. F. Man, A. C. H. Smith, and M. F. A. Harrison, J. Phys. B **26**, 1365 (1993).
[10] M. E. Bannister, D. W. Muller, L. J. Wang, M. S. Pindzola, D. C. Griffin, and D. C. Gregory, Phys. Rev. A **38**, 38 (1988).
[11] M. H. Chen and K. J. Reed, Phys. Rev. A **47**, 1874 (1993).
[12] N. R. Badnell and M. S. Pindzola, Phys. Rev. A **47**, 2937 (1993).
[13] N. R. Badnell, D. C. Griffin, and M. S. Pindzola, J. Phys. B **24**, L275 (1991).
[14] M. S. Pindzola, T. W. Gorczyca, N. R. Badnell, D. C. Griffin, M. Stenke, G. Hofmann, B. Weissbecker, K. Tinschert, E. Salzborn, A Müller, and G. H. Dunn, Phys. Rev. A **49**, 933 (1994).
[15] D. C. Griffin, M. S. Pindzola, and N. R. Badnell, J. Phys. B **24**, L621 (1991).
[16] S. M. Younger, Phys. Rev. A **22**, 111 (1980).
[17] M. S. Pindzola, D. C. Griffin, and C. Bottcher, in *Atomic Processes in Electron-Ion and Ion-Ion Collisions*, Vol. 145 of *NATO Advanced Study Institute, Series B: Physics*, edited by F. Brouillard (Plenum, New York, 1986), p. 75.
[18] M. S. Pindzola, D. C. Griffin, and C. Bottcher, Phys. Rev. A **33**, 3787 (1986).
[19] R. D. Cowan, *The Theory of Atomic Structure and Spectra* (University of California, Berkeley, 1981).
[20] M. S. Pindzola, D. C. Griffin, and C. Bottcher, Phys. Rev. A **39**, 2385 (1989).
[21] M. A. Hayes and M. J. Seaton, J. Phys. B **10**, L573 (1977).
[22] N. R. Badnell, M. S. Pindzola, and D. C. Griffin, Phys. Rev. A **43**, 2250 (1991).
[23] M. S. Pindzola, N. R. Badnell, and D. C. Griffin, Phys. Rev. A **46**, 5725 (1992).
[24] N. R. Badnell, D. C. Griffin, T. W. Gorczyca, and M. S. Pindzola, Phys. Rev. A **48**, 2519 (1993).
[25] P. G. Burke and W. D. Robb, in *Advances in Atomic and Molecular Physics*, edited by D. R. Bates and B. Bederson (Academic Press, New York, 1975), Vol. 11, pp. 143–214.
[26] K. A. Berrington, P. G. Burke, K. Butler, M. J. Seaton, P. J. Storey, and Y. Yan, J. Phys. B **20**, 6379 (1987).
[27] C. Froese Fischer, Comput. Phys. Commun. **64**, 369 (1991).
[28] A. Hibbert, Comput. Phys. Commun. **1**, 359 (1970); **2**, 180 (1971).
[29] C. Froese Fischer, *The Hartree-Fock Method for Atoms* (Wiley, New York, 1977).
[30] M. E. Bannister, X. Q. Guo, and T. M. Kojima, preceding paper, Phys. Rev. A **49**, 4676 (1994).
[31] K. A. Berrington, J. Phys. B **18**, L395 (1985).
[32] C. Bottcher, D. C. Griffin, and M. S. Pindzola, J. Phys. B **16**, L65 (1983).
[33] D. C. Griffin, M. S. Pindzola, and C. Bottcher, Phys. Rev. A **36**, 3642 (1987).
[34] M. S. Pindzola, D. C. Griffin, and C. Bottcher, Phys. Rev. A **41**, 1375 (1990).
[35] R. D. Cowan and D. C. Griffin, J. Opt. Soc. Am. **66**, 1010 (1976).